A density functional theory study of the reconstruction of gold (111) surfaces

Torres, Edmanuel; Dilabio, Gino A.

Publisher's version / Version de l'éditeur:
https://doi.org/10.1021/jp411368v
The Journal of Physical Chemistry C, 118, 29, pp. 15624-15629, 2014-07-04

THE JOURNAL OF PHYSICAL CHEMISTRY C

Article

pubs.acs.org/JPCC

A Density Functional Theory Study of the Reconstruction of Gold (111) Surfaces

Edmanuel Torres*[,†,‡,∥] and Gino A. DiLabio[†,§]

[†]National Institute for Nanotechnology, National Research Council of Canada, 11421 Saskatchewan Drive, Edmonton, Alberta, Canada T6G 2M9

[‡]Faculty of Basic Sciences, Universidad Tecnológica de Bolívar, Cartagena, Colombia

[§]Department of Chemistry, University of British Columbia, Okanagan Campus, Fipke 357, 3247 University Way, Kelowna, British Columbia, Canada V1V 1V7

ABSTRACT: We studied $(p \times \sqrt{3})$ gold (111) surface reconstructions within the DFT/PW91 approximation. Our findings clearly show that the reconstruction is energetically favorable in unreconstructed surfaces equal to or larger than the unit cell of the final reconstructed surface. Reconstructions in surfaces smaller than ∼2.95 nm in the $[1\bar{1}0]$ direction are not more stable than the unreconstructed surface, and this may explain why $(p \times \sqrt{3})$ type reconstructions have not been observed in subnanometer gold particles. We found that reconstructions with $(22 \times \sqrt{3})$ and $(23 \times \sqrt{3})$ unit cells, usually reported in experiments, are isoenergetic.

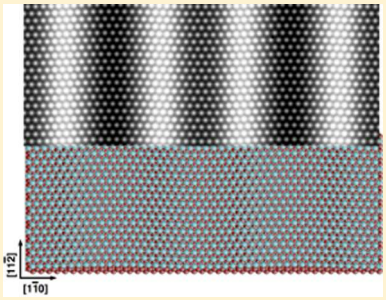

INTRODUCTION

Gold is one of the most widely used metal substrate/electrode materials in research studies and technological applications. Bulk gold has a face centered cubic (fcc) crystal structure, it is a highly inert metal that rarely forms oxides, and it does not strongly react with the atmosphere or with a large number of substances. This high tolerance to the environment is of practical convenience for conducting experiments and for industrial applications.[1,2] By virtue of these characteristics, it is relatively simple to prepare a clean, flat, and stable gold surface. The most common method for doing so it is by thin film growth on silicon wafers, glass, mica, or plastic substrates. Gold surfaces are regularly prepared by vapor deposition methods, electrodeposition, or electroless deposition.[2−4] After annealing, the surface is nearly flat and exhibits terraces of the most stable (111) surface. The crystalline quality, the number of non-(111)-oriented crystallites, the density of defects, etc., can vary substantially, depending on the evaporation conditions, the thermal treatment, and other parameters.[5]

It is well-known that the clean Au(111) surfaces undergo reconstruction[3,6−11] and, in fact, so far it is the only known (111) surface of a fcc metal to do so at room temperature.[7,10,12] Reconstruction of the (111) surface is not observed for Pd, Cu, and Ag.[7] Early electron diffraction studies by Finch et al. reported anomalous patterns,[6] which subsequent transmission electron microscopy[7] and transmission electron diffraction[3] suggested were due to the formation of a $(22 \times \sqrt{3})$ reconstructed superstructure with respect the hexagonal lattice of the gold (111) surface. Later scanning tunneling microscopy studies performed on clean Au(111) reported a stacking-fault reconstruction with $(22 \times \sqrt{3})$[10] and $(23 \times \sqrt{3})$[9] unit cells, resulting in a compression of the topmost layer of atoms along the $[1\bar{1}0]$ direction of 4.20% and 4.55%, respectively, in which the 23[10] or 24[9] atoms in the topmost layer sit on 22 or 23 atoms of the under gold atom layer, respectively. Within the unit cell, the atom positions make a transition from face-centered cubic (fcc) through bridged sites (brg) to hexagonal close-packed (hcp) positions and back through brg to fcc. The helium spin−echo (HeSE) technique was recently applied to the Au(111) surface and indicated a $(23 \times \sqrt{3})$ superstructure.[13]

The role of the reconstructed gold surface on processes like adsorption are likely to be very important but are difficult to study by simulations owing to the computational demand associated with the required unit cell. Early computational studies of the reconstruction have been made by means of molecular dynamics simulations.[14,15] The studies by Ercolessi et al. found the $(11 \times \sqrt{3})$ reconstructed surface to be the most stable relative to the unreconstructed surface. Nonrelativistic density functional theory (DFT)[16,17] studies of the $(22 \times \sqrt{3})$ reconstructed surface have appeared in the literature, in plane-wave investigations using the PW91[18] and PBE[19] functionals. However, to date, we know of no attempt to predict the most stable reconstructed structure from first-principles DFT.

In this work we present a comprehensive DFT/PW91 study of the $(p \times \sqrt{3})$ reconstructions of the Au(111) surface, with p being the slab size index. We considered surface reconstructions for $p \geqslant 4$ and $p \leqslant 25$, thereby testing the ability of a commonly used DFT-based approach to predict the reconstruction of a metal of broad importance.

Received: November 19, 2013
Revised: June 24, 2014
Published: July 4, 2014

COMPUTATIONAL DETAILS

All calculations were performed using DFT[16,17] as implemented in the program VASP.[20] The exchange and correlation energy was described by the generalized gradient approximation (GGA) functional of Perdew and Wang (PW91).[21] The ion−electron interactions, including scalar relativistic effects, were described by projector augmented-wave (PAW) pseudopotentials.[22,23] A kinetic energy cutoff of 400 eV for the plane wave basis set was used for the final results. The Brillouin zone integrations were performed using Monkhorst−Pack k-point grids[24] and did not include the Γ-point.

Surfaces were modeled by periodic supercells, consisting of 4 layers of gold (111) slabs separated by vacuum equivalent to 10 layers in the [111] direction to avoid spurious interactions between unit cell images. The unreconstructed surfaces were modeled by $(p \times \sqrt{3})$ slabs constructed by stacking p times the $(1 \times \sqrt{3})$ unit cell along the $[1\bar{1}0]$ direction with a surface area of 1.509 nm^2.

To develop the structures of the reconstructed surfaces, we utilized the following steps: (1) Initially, the unreconstructed $(4 \times \sqrt{3})$ and $(6 \times \sqrt{3})$ slabs were built and optimized. The reconstructions were generated by accommodating one extra gold atom in each row of the topmost layer, followed by a preoptimization of the slab using a $(1 \times 2 \times 1)$ k-point grid and then reoptimized using a $(2 \times 8 \times 1)$ grid. (2) Upon completion of the preoptimization in step 1, a $(1 \times \sqrt{3})$ unit cell was added to the end of the slab, p, along the $[1\bar{1}0]$ direction, thus building the $p + 1$ reconstructed slab. (3) The positions of the atoms in the layer were rescaled to be equally spaced in the $[1\bar{1}0]$ direction. (4) The geometry was fully optimized and the process was repeated from step 2 with the $p = 6$ up to $p = 25$.

We selected a set of structures for subsequent optimizations and performed a stepwise increase of the k-point sampling using the following sequence of grids: $(2 \times 8 \times 1)$, $(4 \times 8 \times 1)$, $(6 \times 8 \times 1)$, and $(8 \times 8 \times 1)$. In all cases, the two bottom gold layers were fixed in positions using the lattice constant obtained from the modeling of bulk gold, i.e., $a = 4.17$ Å. The first-order Methfessel−Paxton electron smearing scheme with $\sigma = 0.2$ eV was found to keep the entropic contribution to the energy from exceeding 0.1 meV/atom, thereby providing appropriate parameters for structure optimizations. All the structures were optimized using a maximum residual force convergence criterion of 0.01 eV/Å. Energies were converged to within ±0.1 meV. In order to avoid systematic errors, the same level of computation was used for the unreconstructed and reconstructed slabs in all the calculations.

Following the preliminary optimizations described above, we selected the set of structures for $p = 4$, 6, 7, 10, 11, 12, 14, 16, 18, 20, 22, 23, 24, and 25 (hereafter referred to simply as p unit cells) for subsequently more refined calculations. Then, the following simple relation can be employed to compute the surface energy (E_s) within the supercell approach

$$E_s(N_l) = (1/A) \lim_{N_l \to \infty} [E_{slab}(N_l) - N_l E_b] \quad (1)$$

where $E_{slab}(N_l)$ is the total electronic energy obtained from a DFT calculation of the l layers slab. N_l is the total number of atoms. E_b is the bulk energy per atom, and A is the slab surface area. The computed E_s accounts for the surface energies of the two faces of the slab. It is reasonable to compute the E_b as the energy per atom from a separate bulk calculation. However, as it was pointed out by Boettger[25] that, for metals, the accuracy of the reconstruction energy evaluated using eq 1 may be in fact deteriorated by using an independent bulk reference as a result of quantum size effects.[26] Therefore, methods to obtain accurate surface energies from thin slabs calculations have been proposed.[25,27,28] See ref 29 for a recent review of surface energy calculations.

In this work, we have used the approach described in the ref 27, in which the linear relation between the total energy, $E_{slab}(N_l)$, given by

$$E_{slab}(N_l) \approx AE_s'(N_l) + N_l E_b' \quad (2)$$

can be fitted to a sequence of total energy calculations of slabs with l layers to obtain E_s' and E_b'. This relation was found to be reasonable for very thin slabs.[27]

As the number of atoms required for the modeling of the gold surface reconstructions increases very quickly with p, the relaxation of both faces is not practical in this study. To keep the computational cost practical, we performed relaxation only of the top face. Therefore, in order to obtain the surface energy E_s of the relaxed face for the slab p, we excluded the surface energy of the frozen face in the following manner

$$E_s = E_s(N) - \frac{1}{2}E_f(N) \quad (3)$$

where E_s represents the combined surface energies of the reconstructed (or unreconstructed) face and the frozen face. E_f is the surface energy of the unreconstructed frozen slab, and the coefficient $^1/_2$ accounts for the two equivalent faces. The surface energies E_s and E_f can be obtained through eqs 1 or 2. In this approach E_f is obtained from a single point energy calculation of a frozen slab.

In order to assess the stability of the reconstructed surfaces, we have also evaluated the energy required to create the reconstructed surface from the unreconstructed surface ΔE and two atoms taken from the bulk reservoir as follows:

$$\Delta E = E_r - E_u - 2E_b \quad (4)$$

Here E_r and E_u are the total DFT electronic energies for the reconstructed and the unreconstructed slabs, respectively. E_b is the energy of a bulk atom (vide infra).

RESULTS AND DISCUSSION

We have first evaluated the accuracy of our results with respect the slab thickness. For this purpose, we have calculated energies for the $p = 12$, 16, and 22 slabs with $l = 4$, 5, and 6 layers, using 400 eV cutoff energies and a $(8 \times 8 \times 1)$ k-point mesh. The surface energies obtained using eqs 2 and eq 1 are summarized in Table 1.

In order to evaluate the surface energies $E_{s,l}$ in Table 1, we used $E_b = -3.2019$ obtained from the average of gold atom bulk energies listed in Table 1. We found that E_s' energies changed by ∼0.01 eV when a 350 eV cutoff was used. Table 1 clearly shows that surfaces energies obtained using using eq 1 are in

Table 1. E_b' (eV) and E_s' (eV/nm^2) are the Results from the Linear Fitting of the Series to Eq 2[a]

p	E_b'	E_s'	$E_{s,4}$	$E_{s,5}$	$E_{s,6}$
12	−3.2017	4.1716	4.1941	4.1885	4.2035
16	−3.2020	4.0767	4.0836	4.0796	4.0862
22	−3.2020	4.1213	4.1009	4.0839	4.0890

[a] $E_{s,l}$ are the surface energies for slabs with l layers using eq 1.

dx.doi.org/10.1021/jp411368v | J. Phys. Chem. C 2014, 118, 15624−15629

Table 2. Mean Absolute Error (MAE, eV) for ΔE Using a 350 eV with Respect to the Reconstruction Energies Obtained Using a $(8 \times 8 \times 1)$ *k*-Point Grid and a 400 eV Energy Cutoff

k-points	$(2 \times 8 \times 1)$	$(4 \times 8 \times 1)$	$(6 \times 8 \times 1)$	$(8 \times 8 \times 1)$
MAE	0.043	0.013	0.006	0.003

close agreement with the energies resulting from the fitting to eq 2. This indicates that there is not a large size effect associated with the use of a gold slab with four layers. Furthermore, the use of eq 1 gives the same trend of surface energies. This provides us with the confidence to use eq 1 and the averaged gold bulk energy E_b for the computation of surface energies using four-layer slabs hereafter.

The mean absolute error (MAE) values of the reconstruction energies ΔE for all the p slabs considered in this work, using a 350 eV energy cutoff for a series of *k*-point grid, are shown in Table 2. The reference values were obtained using a $(8 \times 8 \times 1)$ *k*-point grid and a 400 eV energy cutoff. It is clear that the error substantially increases with the reduction of the *k*-point grid size. Therefore, we recommend the use of a $(4 \times 8 \times 1)$ *k*-point grid with a 350 eV cutoff to obtain results to within ∼0.01 eV. Nevertheless, convergence was achieved with a $(8 \times 8 \times 1)$ *k*-point grid and 400 eV energy cutoff. Thus, we employed these parameters in the remaining calculations presented herein.

The surface and reconstruction energies as a function of p are listed in Table 3. The surfaces energies of reconstructed slabs

Table 3. Surface (eV/nm^2) for the Reconstructed (E_s^r) and Unreconstructed (E_s^u) Surfaces, and Reconstruction Energies (ΔE)

p	E_s^r	E_s^u	ΔE (eV)
4	6.080	4.409	1.036
6	7.110	4.429	2.469
7	5.768	4.421	1.471
10	4.423	4.415	0.080
11	4.283	4.416	−0.145
12	4.194	4.415	−0.318
14	4.119	4.415	−0.528
16	4.084	4.416	−0.693
18	4.085	4.416	−0.776
20	4.091	4.417	−0.846
22	4.101	4.415	−0.890
23	4.114	4.416	−0.888
24	4.124	4.413	−0.879
25	4.134	4.411	−0.873

for p = 4−10 are higher than those for the unreconstructed slabs. The lowest surface energies are found for the p = 16 and 18 reconstructed slabs. Nevertheless, the surface energy slowly increases for p > 16.

Considering the reconstruction energies ΔE as a function of unit cell p value paints a different picture. The reconstruction in a unit cells p = 10 is endothermic by this measure, as are those with p < 10, indicating that the unreconstructed surface is, at best, energetically metastable.

As can be seen in Figure 1, which shows the reconstruction energies (ΔE) as a function of the slab index size (p), values of ΔE decrease monotonically with increasing p, reaching a minimum at p = 22 and 23. These reconstructions are more stable in energy by −0.89 eV relative to the unreconstructed surface. Remarkably, only 0.01 eV separates the reconstruction energies associated with p = 22 and 23. The minimum in the

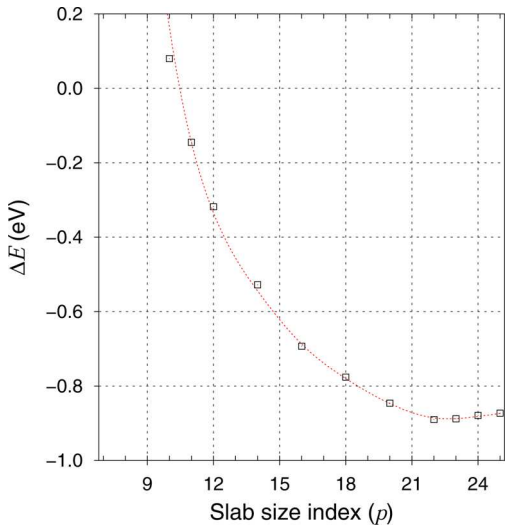

Figure 1. Reconstruction energy ΔE as a function of the slab size index p.

energies of surface reconstructions found at p = 22 ± 1 are in agreement with the reported size of the reconstructed unit cell found in experiments.

We observed that our computed reconstruction energy for p = 22 of −0.89 eV is closer to the value of −1.14 eV reported in ref 19 than it is to the value of 0.43 eV reported in ref 18. Our expectation is that the lower values obtained in ref 18 are partly due the small basis set defined by their applied energy cutoff.

Table 3 indicates that the reconstruction may result from a spontaneous stabilization mechanism initiated within unreconstructed surfaces, until the surface reaches the final most stable reconstructed surface. From Figure 1 it can be seen that reconstructions to a particular p = 22 ± 1 value may be initiated within surface regions larger or equal in size to the associated unit cell of that p value.

The bottom in Figure 1 is very flat, suggesting that reconstructions for p = 21−25 may exist. However, reconstructions with unit cells smaller than p = 22 or larger than p = 23 have not been observed in experiments. On the other hand, reconstructions for p = 22 and 23 unit cells have been widely reported in experiments at room temperature.[3,8−13] Interestingly, we have obtained very close ΔE for these two surfaces, with a difference of only 2 meV. This suggest that the barrier for the phase transition may have an important role for the stability of the p = 22−23 reconstructed surfaces. However, modeling the barriers associated with phase transitions is extremely time-consuming and beyond the scope of this work. For $p \leq 10$, which corresponds to surfaces smaller than 2.95 nm, reconstructions are not favorable, suggesting that, in the absence of other driving forces such as edge boundaries, etc., gold particles on this size scale would not undergo surface reconstructions.

Figure 2 illustrates the initial unreconstructed and final reconstructed p = 23 surfaces. The unreconstructed surface exhibits regular fcc termination of the topmost layer, while the reconstructed surface shows the above-described stacking-fault

dx.doi.org/10.1021/jp411368v | J. Phys. Chem. C 2014, 118, 15624−15629

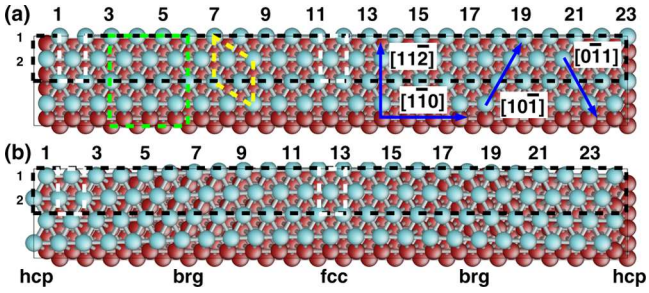

Figure 2. Ball–stick representation of the top view for the $(23 \times 2\sqrt{3})$ unreconstructed (a) and reconstructed (b) unit cells. The topmost layer of atoms are colored bright blue. $(1 \times \sqrt{3})$ unit cells are highlighted by white dotted lines on both surfaces. The $(3 \times 2\sqrt{3})$ and the $(\sqrt{3} \times \sqrt{3})R30°$ are highlighted by green and yellow dotted lines, respectively. Various surface directions are indicated by dark blue arrows.

reconstruction. In general, this stacking-fault model of reconstruction can be obtained in slabs with $p \geq 6$ unit cells.

In order to compare the reconstructed geometries, we evaluated the maximum lateral displacement (D^x_{lat}) in the $[11\bar{2}]$ direction (see Figure 2) and the surface corrugation (D^x_{corr}) for the topmost layer ($x = 1$), for which plenty experimental data are available, and for the second layer ($x = 2$) of the reconstructed gold surfaces. These data are listed in Table 4. We did not find significant variations in structural parameters with the increases in the number of slab layers.

Table 4. Corrugation and Maximum Lateral Displacement, of the Two Top Layers, in the [111] and $[11\bar{2}]$ Directions, Respectively[a]

p	D^1_{lat}	D^1_{corr}	D^2_{lat}	D^2_{corr}
4	0.78	2.16	0.06	0.14
6	0.54	0.11	0.01	0.04
7	0.45	0.17	0.05	0.03
10	0.50	0.11	0.09	0.03
11	0.57	0.10	0.06	0.02
12	0.59	0.10	0.06	0.02
14	0.62	0.10	0.09	0.02
16	0.60	0.08	0.09	0.01
18	0.72	0.08	0.04	0.01
20	0.77	0.08	0.04	0.01
22	0.75	0.08	0.04	0.01
23	0.75	0.08	0.05	0.01
24	0.75	0.08	0.06	0.01
25	0.76	0.09	0.07	0.01

[a]Lengths are in Å.

D_{corr} in Table 4 shows that the corrugation of the top two layers of the gold surface generally increases as the slab size decreases. However, the lateral displacement in the second layer (D^2_{lat}) shows only a weak dependency on the slab size. There are two discernible groups of structures with similar characteristics; those are for $p = 10–12$ and $p = 16–25$. But only those for $p = 16–25$, with $D^1_{lat} \sim 0.8$ Å and $D^1_{corr} \sim 0.08$ Å, show close agreement with the surface corrugation of 0.15 ± 0.4 Å[9] and with the lateral displacement of 0.9 Å[10] reported in experiments. The slab for $p = 4$ exhibits a very different reconstruction as compared with those associated with the other slabs, with the D^1_{corr} value of 2.16 Å being close to the separation of 2.41 Å between planes along the [111] direction in gold bulk.

Figure 3 provides a detailed structural analysis of the topmost layer of the $(23 \times \sqrt{3})$ reconstructed surface. In general, bond

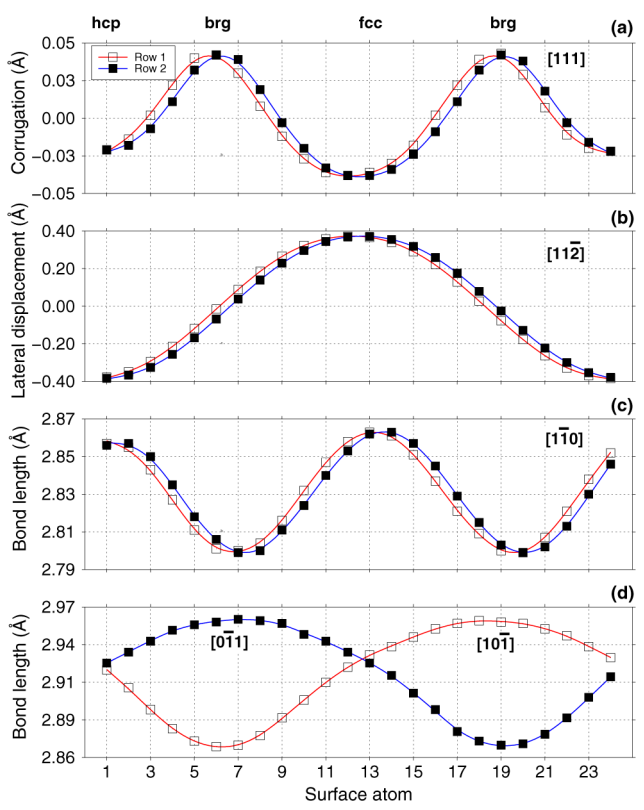

Figure 3. Structural parameters of the topmost layer of the $(23 \times \sqrt{3})$ as a function of the atomic position of each row indicated in Figure 2b. The surface directions are indicated on each plot.

lengths associated with the surface atoms are seen to vary with position, as is expected in response to the reconstruction, and the variability in structural parameters as a function of atom position is smooth.

The corrugation shown in Figure 3a was evaluated using the average height of the surface atoms. The lowest height on the surface occurs at the fcc stacking region. The hcp region is slightly higher by 0.02 Å. We found the highest corrugation in the brg regions, which is in agreement with the results in STM experiments.[9] From Figure 3b, it can be clearly seen that the reconstruction mainly results in a large lateral displacement, visible in Figure 2b. This suggests that the large variations in corrugation in STM experiments may be due to the tunneling conditions used in the experiments in combination with the effects on the electronic structure of the reconstruction.[9,10]

Figure 3c shows that bond lengths between atoms, in the $[1\bar{1}0]$ direction, are 2.86 Å in both the fcc and hcp regions, which is slightly larger compared to a bond length of 2.8 Å in the brg regions. Therefore, atoms are slightly more densely packed near the brg regions. Figure 3d shows that bond lengths change asymmetrically in the $[10\bar{1}]$ and $[0\bar{1}1]$ directions when going from hcp → fcc, beginning with 2.93 Å in the hcp region, then to 2.96 Å ($[10\bar{1}]$) and 2.87 Å ($[0\bar{1}1]$) in the brg region, and back to 2.93 Å the fcc region. When going from fcc → brg this variation is reversed.

dx.doi.org/10.1021/jp411368v | J. Phys. Chem. C 2014, 118, 15624–15629

CONCLUSION

We studied $(p \times \sqrt{3})$ surface reconstructions of the gold (111) surface from $p = 4$ to 25 using the DFT/PW91 approach. Our findings show that for $p > 10$ the reconstruction is energetically more favorable than the unreconstructed surface, and reconstruction to unit cells that have been observed experimentally would be exoergic from larger or equal unit cells. Additionally, the energy cost of formation increases very sharply as the unit cell size decreases below $p = 10$. Therefore, reconstructions in surfaces with dimension of $\leq$2.95 nm are energetically unfavorable. This indicates that the surfaces of small nanoparticles may not undergo reconstruction.

The $(22 \times \sqrt{3})$ and $(23 \times \sqrt{3})$ have been reported in experiments at room temperature. However, we have found that reconstruction energies and structural characteristics for $p = 22-25$ are very similar. In general, structures with $p \geq 10$ were found to be more stable than the unreconstructed ones, suggesting that they may occur. However, their direct observation may require particular experimental conditions, as reported in very few experiments.[12,11]

Surface reconstructions may alter the properties of the gold surface relative to those of unreconstructed gold (111). Therefore, the limitation associated with the use of the unreconstructed gold surface in modeling work should be acknowledged. Processes such as adsorption may also influence the nature of gold (111) surface reconstruction. We suggest that, at a minimum, a $p \geq 14$ unit cell should be used to appropriately model the properties of the gold (111) reconstructed surface.

In summary, we found that the DFT/PW91 approximation is capable of predicting gold (111) surface reconstructions that are in good agreement with the experimentally observed surfaces. The study of the barriers associated with transitions between different structures and the inclusion of thermal energies represent important next steps in understanding the mechanisms associated with surface reconstructions.

AUTHOR INFORMATION

Corresponding Author

*E-mail: eetorres@mit.edu.

Present Address

[‖]Department of Materials Science and Engineering, Massachusetts Institute of Technology, Bldg 13-5005, 77 Massachusetts Ave., Cambridge, MA 02139.

Notes

The authors declare no competing financial interest.

ACKNOWLEDGMENTS

We are extremely grateful to the NanoAlberta for financial support and to WestGrid of Compute Canada for a generous allocation of computing resources.

REFERENCES

(1) Hammer, B.; Norskøv, J. K. Why Gold Is the Noblest of All the Metals. *Nature* **1995**, *376*, 238−240.

(2) Love, J.; Estroff, L.; Kriebel, J.; Nuzzo, R.; Whitesides, G. Self-Assembled Monolayers of Thiolates on Metals as a Form of Nanotechnology. *Chem. Rev.* **2005**, *105*, 1103−1170.

(3) Heyraud, J.; Métois, J. Anomalous 422 Diffraction Spots from {111} Flat Gold Crystallites: (111) Surface Reconstruct Ion and Moiré Fringes Between the Surface and the Bulk. *Surf. Sci.* **1980**, *100*, 519−528.

(4) Emch, R.; Nogami, J.; Dovek, M. M.; Lang, C. A.; Quate, C. F. Characterization of Gold Surfaces for Use As Substrates in Scanning Tunneling Microscopy Studies. *J. Appl. Phys.* **1989**, *65*, 79−84.

(5) Schreiber, F. Structure and Growth of Self-Assembling Monolayers. *Prog. Surf. Sci.* **2000**, *65*, 151−257.

(6) Finch, G. I.; Quarrell, A. G.; Wilman, H. Electron Diffraction and Surface Structure. *Trans. Faraday Soc.* **1935**, *31*, 1051−1080.

(7) Yagi, K.; Takayanagi, K.; Kobayashi, K.; Osakabe, N.; Tanishiro, Y.; Honjo, G. Surface Study by an {UHV} Electron Microscope. *Surf. Sci.* **1979**, *86*, 174−181.

(8) Harten, U.; Lahee, A. M.; Toennies, J. P.; Wöll, C. Observation of a Soliton Reconstruction of Au(111) by High-Resolution Helium-Atom Diffraction. *Phys. Rev. Lett.* **1985**, *54*, 2619−2622.

(9) Wöll, C.; Chiang, S.; Wilson, R. J.; Lippel, P. H. Determination of Atom Positions at Stacking-Fault Dislocations on Au(111) by Scanning Tunneling Microscopy. *Phys. Rev. B* **1989**, *39*, 7988−7991.

(10) Barth, J. V.; Brune, H.; Ertl, G.; Behm, R. J. Scanning Tunneling Microscopy Observations on the Reconstructed Au(111) Surface: Atomic Structure, Long-Range Superstructure, Rotational Domains, and Surface Defects. *Phys. Rev. B* **1990**, *42*, 9307−9318.

(11) Tao, N. J.; Lindsay, S. M. Observations of the $22 \times \sqrt{3}$ Reconstruction of Au(111) under Aqueous Solutions Using Scanning Tunneling Microscopy. *J. Appl. Phys.* **1991**, *70*, 5141−5143.

(12) Sandy, A. R.; Mochrie, S. G. J.; Zehner, D. M.; Huang, K. G.; Gibbs, D. Structure and Phases of the Au(111) Surface: X-ray-Scattering Measurements. *Phys. Rev. B* **1991**, *43*, 4667−4687.

(13) McIntosh, E. M.; Kole, P. R.; El-Batanouny, M.; Chisnall, D. M.; Ellis, J.; Allison, W. Measurement of the Phason Dispersion of Misfit Dislocations on the Au(111) Surface. *Phys. Rev. Lett.* **2013**, *110*, 086103.

(14) Ercolessi, F.; Bartolini, A.; Garofalo, M.; Parrinello, M.; Tosatti, E. Au Surface Reconstructions in the Glue Model. *Surf. Sci.* **1987**, *189190*, 636−640.

(15) Ravelo, R.; El-Batanouny, M. Molecular-Dynamics Study of the Reconstructed Au(111) Surface: Low Temperature. *Phys. Rev. B* **1989**, *40*, 9574−9589.

(16) Hohenberg, P.; Kohn, W. Inhomogeneous Electron Gas. *Phys. Rev.* **1964**, *136*, B864−B871.

(17) Kohn, W.; Sham, L. J. Self-Consistent Equations Including Exchange and Correlation Effects. *Phys. Rev.* **1965**, *140*, A1133−A1138.

(18) Wang, Y.; Hush, N. S.; Reimers, J. R. Simulation of the Au(111)-$(22 \times \sqrt{3})$ Surface Reconstruction. *Phys. Rev. B* **2007**, *75*, 233416.

(19) Hanke, F.; Björk, J. Structure and Local Reactivity of the Au(111) Surface Reconstruction. *Phys. Rev. B* **2013**, *87*, 235422.

(20) Kresse, G.; Furthmüller, J. Efficient Iterative Schemes for Ab Initio Total-Energy Calculations Using a Plane-Wave Basis Set. *Phys. Rev. B* **1996**, *54*, 11169−11186.

(21) Perdew, J. P.; Wang, Y. Accurate and Simple Analytic Representation of the Electron-Gas Correlation Energy. *Phys. Rev. B* **1992**, *45*, 13244−13249.

(22) Blöchl, P. E. Projector Augmented-Wave Method. *Phys. Rev. B* **1994**, *50*, 17953−17979.

(23) Kresse, G.; Joubert, D. From Ultrasoft Pseudopotentials to the Projector Augmented-Wave Method. *Phys. Rev. B* **1999**, *59*, 1758−1775.

(24) Monkhorst, H. J.; Pack, J. D. Special Points for Brillouin-Zone Integrations. *Phys. Rev. B* **1976**, *13*, 5188−5192.

(25) Boettger, J. C. Nonconvergence of Surface Energies Obtained from Thin-Film Calculations. *Phys. Rev. B* **1994**, *49*, 16798−16800.

(26) Boettger, J. C. Persistent Quantum-Size Effect in Aluminum Films up to Twelve Atoms Thick. *Phys. Rev. B* **1996**, *53*, 13133−13137.

(27) Fiorentini, V.; Methfessel, M. Extracting Convergent Surface Formation Energies from Slab Calculations. *J. Phys.: Condens. Matter* **1998**, *10*, 895.

(28) Boettger, J. C.; Smith, J. R.; Birkenheuer, U.; Rösch, N.; Trickey, S. B.; Sabin, J. R.; Apell, S. P. Extracting Convergent Surface

Formation Energies from Slab Calculations. *J. Phys.: Condens. Matter* **1998**, *10*, 893.
(29) Frankcombe, T. J.; Løvvik, O. M. The Crystal Structure and Surface Energy of $NaAlH_4$: A Comparison of DFT Methodologies. *J. Phys. Chem. B* **2006**, *110*, 622−630.